Chemical Physics Letters 479 (2009) 173–183

Contents lists available at ScienceDirect

Chemical Physics Letters

journal homepage: www.elsevier.com/locate/cplett

FRONTIERS ARTICLE

Specific ion adsorption at the air/water interface: The role of hydrophobic solvation

Dominik Horinek [a,*], Alexander Herz [a], Lubos Vrbka [b], Felix Sedlmeier [a], Shavkat I. Mamatkulov [a,c], Roland R. Netz [a]

[a] Physik Department, Technische Universität München, 85748 Garching, Germany
[b] Institut für Physikalische und Theoretische Chemie, Universität Regensburg, 93040 Regensburg, Germany
[c] Heat Physics Department of Uzbekistan Academy of Sciences, 28 Katartalstr., 700135 Tashkent, Uzbekistan

ARTICLE INFO

Article history:
Received 24 July 2009
In final form 24 July 2009
Available online 28 July 2009

ABSTRACT

Classical force fields for molecular simulations of aqueous electrolytes are still controversial. We study alkali and halide ions at the air/water interface using novel non-polarizable force fields that were optimized based on bulk thermodynamics. In qualitative agreement with polarizable force-field simulations, ion repulsion from the interface decreases with increasing ion size. Iodide is even enhanced at the interface, which is rationalized by hydrophobic solvation at the interface, but exhibits a smaller surface propensity than in previous polarizable simulations. Surprisingly, lithium is less repelled than other cations because of its tightly bound hydration shell. A generalized Poisson–Boltzmann approach that includes ionic potentials of mean force from simulation almost quantitatively matches experimental interfacial tension increments for 1 molar sodium halides and alkali chlorides. We conclude that properly optimized non-polarizable force fields are transferable to interfacial environments and hold the potential for unravelling ion-specific effects even in biological situations involving peptidic surfaces.

1. Introduction

The behavior of ions at the air/water interface is a classic problem of physical chemistry with many important implications and still puzzling questions [1]. Experiments on ion adsorption at the surface of water are notoriously difficult, specially for low salt concentrations, because of the susceptibility to small traces of surface-active contaminants. On the other hand, surface tension measurements allow to directly gain information of the surface activity of salts and give reliable account of the interfacial thermodynamics [2]. Experimentally, it is observed that salt addition to water typically increases the surface tension, which implies that there is a negative surface excess (i.e. depletion) in the sum of the density profiles of anions and cations. However, there have been experiments that indicate an increased density of some anions in the interfacial layer. The majority of these experiments is based on sum frequency generation [3] or second harmonic generation nonlinear optical techniques [4]. Direct evidence of iodide being enhanced at the air/water interface was obtained with a completely different experimental probe using grazing incidence X-ray fluorescence [5].

In their classical model, Onsager and Samaras identified the interfacial forces acting on ions with electrostatic image forces, which repel all ions from the interface between water ($\epsilon_r = 78$) and air ($\epsilon_r = 1$) [6]. This theory relies on a continuum description of water and cannot explain or describe ion-specific effects. Since then, analytic models were refined and generalized to include effects due to ion size [7] or dispersion interactions [8] and thus can allow to treat ion-specific effects on a heuristic level. Using molecular simulations, it was recognized that the discrete nature of the water molecules crucially determines the molecular structure in the interfacial region [9]. As a consequence, solvation forces acting on ions in the interfacial region cannot be described by simple continuum models [10]. Nevertheless, information on the properties of such complex systems are accessible by molecular simulation methods, either Monte Carlo or molecular dynamics (MD), employing suitable atomistic force fields. Soon after the seminal works on the simulation of water at a hydrophobic surface [11] and at the air/water interface [9], a simulation of a sodium ion at the air/water interface was reported [12]. Polarizable force fields for ions and water were applied to bulk water [13,14] and ions in small water clusters [15]. During the last decade, there has been a tremendous amount of simulation work on ions at interfaces. Starting with the work of Jungwirth and Tobias [16], such polarizable force fields for ions and water have been extensively applied for studies of ions at the air/water interface [17,18], and have also been used for the study of ions at a solid hydrophobic self-assembled monolayer [10]. The common rationale behind using polarizable force fields is the idea that ion affinity for an interface arises from the favorable interaction of the polarizability of an ion [18] with the interfacial electric field due to the mean orientation of interfacial water molecules [19,11]. This view was supported by

* Corresponding author.
E-mail address: dominik.horinek@ph.tum.de (D. Horinek).

0009-2614/$ - see front matter © 2009 Elsevier B.V. All rights reserved.
doi:10.1016/j.cplett.2009.07.077

simulations where the ad hoc neglect of polarizability suppressed the adsorption of iodide at the air/water interface [20]. On the other hand, in subsequent simulations it was shown that even non-polarizable anions are attracted to hydrophobic interfaces, if their effective radius is chosen large enough [21–23]. It transpires that in silicon there are many different mechanisms that can drive ions to the air/water interface, but it is not exactly clear which mechanism is actually responsible for iodide's observed interfacial activity. A systematic study of anion affinity to the air/water interface using thermodynamically consistent force fields, which would be able to answer this question, has not been reported so far.

The required input for any molecular simulation is the force field acting on all atoms, based on which the simulation generates information about, e.g. the solvation forces present in the system. The underlying atomistic potential is either a classical force field that relies on parameterized functions or a quantum-mechanically derived potential, which is derived by an approximate method of quantum chemistry. Both types of potentials have disadvantages: quantum-chemical methods are relatively accurate, but their computational demand poses a serious limitation for the accessible simulation times and system sizes (for a current state-of-the-art ab initio MD simulation of a solvated ion at a graphite/water interface see Ref. [24]), and converged spatial distribution functions of complex systems cannot be expected even if sophisticated sampling techniques are applied. Furthermore, density functional theory methods, which are particularly popular in ab initio MD applications, should be considered with care in liquid state simulations, because they give a rather poor description of dispersion forces. Simulations based on classical force fields are able to yield converged potentials of mean force, but all results obtained depend on the force field employed and thus inherit all inadequacies of that force field. The functional form and the numerical parameters of a force field are generally chosen such that a given set of experimental properties (or quantum mechanical energies) are reproduced as well as possible. Therefore, classical simulation results should generally be interpreted with great care, and it is good practice to evaluate a force field's transferability by comparison to reliable experimental data that go beyond the particular set of experimental data that has been used to optimize the force field in the first place.

The common wisdom concerning simulations of ions at interfaces is that the ion force fields should be optimized to correctly reproduce ionic bulk properties. In the vapor phase, this is trivial for mononuclear ions, and in the aqueous phase, an optimization strategy could involve thermodynamic properties like the solvation free energy or the solvation entropy. Standard non-polarizable ion force fields require the optimization of the two Lennard-Jones parameters, the diameter σ_{IW} and the interaction strength ε_{IW}, for polarizable models a third parameter, the polarizability α, needs to be optimized. Clearly, the solvation free energy by itself is not sufficient for the simultaneous optimization of two or three parameters. Recently, we have systematically studied the solvation properties of monovalent non-polarizable cations and anions in SPC/E water [25] as a function of the ion-water Lennard-Jones parameters σ_{IW} and ε_{IW} [26]. In that work, we have calculated the solvation free energy ΔG_{solv}, the solvation entropy ΔS_{solv}, and R_1, the first maximum of the ion-oxygen radial distribution function (RDF), on a 2D grid in the $(\sigma_{IW}, \varepsilon_{IW})$-plane and provided analytical fitting functions for these data. Thus, we constructed global surfaces of ΔG_{solv}, ΔS_{solv}, and R_1, for anions and cations. It turns out that the direct optimization of ion parameters for single ions is hampered by large uncertainties of the electrostatic potential jump at the air/water interface [27]. As a way out, we chose one reference ion (chloride described by the Smith–Dang parameters [28]), and optimized the other ions by reproducing the sums of experimental solvation free energies and entropies of neutral ion pairs (for the alkali cations) and by reproducing the differences of experimental free energies and entropies of like charged ion pairs (for the halide anions). Obviously, these sums and differences do not depend on the water surface potential. Thus, we obtain three curves for every ion that demark the values of σ_{IW} and ε_{IW} that reproduce the experimental values of ΔG_{solv}, ΔS_{solv}, and R_1. In Figs. 1 and 2, these curves are shown for halide anions and for alkali cations as solid, broken and dotted lines, respectively. The symbols denote the optimal parameters we suggest. For Cl, Br, and I, the solid and broken lines cross, the loci of which define the optimal parameter values according to our optimization strategy. For Br, the crossing point is not too far from the dotted line (corresponding to the experimental value of R_1 for Br), meaning that the thermodynamically optimized Br force field also gets the solvation structure quite right. By choosing Cl as the reference ion, solid and broken lines for Cl by construction meet at one point, the fact that the dotted line crosses at the same location is an important validation of the Cl force field. For iodide, the three lines

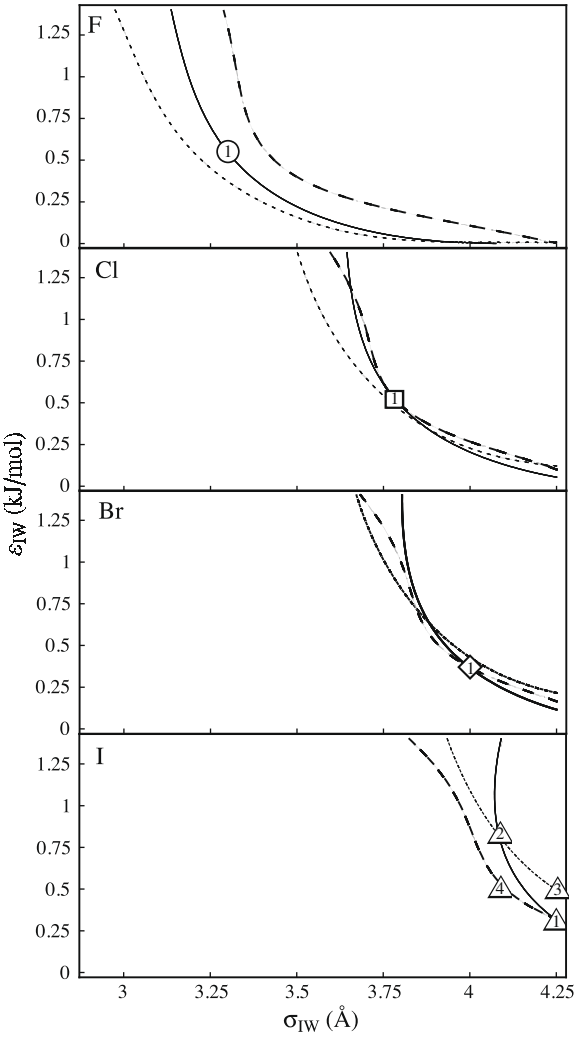

Fig. 1. Scheme of the anion parameter optimization. The lines show combinations of σ_{IW} and ε_{IW} that reproduce the experimental difference of the solvation free energy ΔG_{solv} relative to Smith–Dang chloride [28] (full line), the experimental difference of the solvation entropy ΔS_{solv} relative to Smith–Dang chloride (dashed line), and the position of the first maximum in the ion-oxygen RDF (dotted line). All curves are based on analytical fitting functions. The symbols show our previously optimized parameters [26], which are given in Table 1. Three additional trial parameter sets for iodide are shown. Set 1 is our previously optimized set that reproduces the solvation free energy and the solvation entropy. Set 2 reproduces the solvation free energy and the first maximum of the ion-oxygen RDF. Set 3 reproduces only the first maximum of the ion-oxygen RDF. Set 4 reproduces only the solvation entropy.

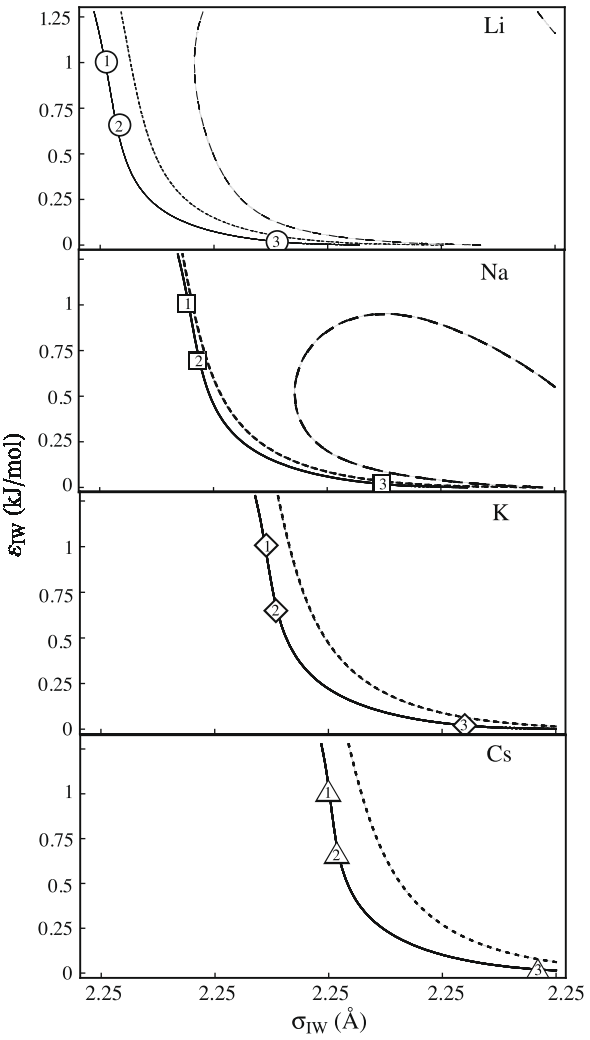

Fig. 2. Cation parameter optimization. The full lines show combinations of σ_{IW} and ε_{IW} that reproduce the sum of experimental solvation free energies, ΔG_{solv}, of the given cation and chloride when used in conjunction with the Smith–Dang parameters for chloride [28]. The sum of experimental solvation entropies ΔS_{solv} is reproduced by the dashed lines, and the position of the experimental first maximum in the ion-oxygen RDF are shown as dotted lines. All curves are based on analytical fitting functions. The symbols show our previously optimized parameters [26] listed in Table 1.

do not simultaneously meet, the point where the lines of ΔG_{solv} (solid line) and ΔS_{solv} (broken line) cross was chosen as the optimal parameter set, denoted by '1', but we also consider in this Letter alternative optimization strategies (leading to the force fields denoted by 2, 3, and 4). For fluoride, there is no crossing point, and the point that reproduces ΔG_{solv} exactly and gives the smallest error in ΔS_{solv} was chosen. For the cations, no crossing points at all are obtained. Therefore, an unequivocal optimization of ε_{IW} and σ_{IW} is not possible just based on single-ion bulk properties. We thus choose three arbitrary values of ε_{IW} (1.00, 0.65, and 0.02 kJ/mol) and determine the respective values of σ_{IW} based on the free energy of solvation curve (solid line). For every cation, we thus end up with three parameter sets, labelled 1, 2, and 3 in Fig. 2, which we use in the interfacial simulations. All parameter sets are listed in Table 1.

Simple point charge models for water like SPC/E and associated ion parameters are nothing but a crude approximation of the forces acting in electrolytes. One possible improvement is the inclusion of atomic polarizabilities. Ions, like any molecular or atomic species, acquire an induced dipole moment in an electric field. In a quantum-chemical framework, the value of the ionic polarizability can be directly obtained from the response of the molecular wavefunction to an external electric field [29]. In a classical simulation, electronic polarization can be taken into account by including parameterized atomic polarizabilities in the force field. In principle, such polarizable force fields have the potential to be closer to the full quantum chemical description of molecular systems; however, two severe drawbacks have so far prevented polarizable force fields from reaching their full potential. As explained above, even the rational optimization of the two Lennard-Jones parameters for non-polarizable ionic force fields based on thermodynamic bulk properties is not straightforward. A global optimization of ionic polarizable force fields has not been attempted so far, but it seems plausible that the addition of a third parameter in the optimization procedure further increases the complexity and ambiguity. In the supplementary information, we actually show that a polarizable ionic force field that was recently used for the simulation of ion-specificity at an alkane self-assembled monolayer/water interface [10], is inferior to properly optimized non-polarizable ionic force fields when applied to bulk solvation properties (see Appendix). Secondly, polarizable force fields based on induced point dipoles can show a polarization catastrophe: the iterative procedure that self-consistently determines the induced dipoles diverges for too large atomic polarizabilities. As shown in the supplement, if a cutoff is used to regularize this divergence, another parameter is introduced into the problem (see Appendix).

In this Letter we study the transferability of non-polarizable ionic force fields that have been optimized in bulk (as described above) to an interfacial adsorption scenario. Specifically, we consider the adsorption of halide and alkali ions to the air/water interface. We present extensive single-ion simulations, from which we extract single-ion interfacial potentials of mean force (PMFs). Feeding those PMFs into a generalized mean-field Poisson–Boltzmann (PB) approach, we calculate ionic density profiles, ionic surface excesses and interfacial tension increments. We validate the generalized PB approach by explicit MD simulations at salt concentration of 0.85 mol/l and find satisfactory agreement for the density profiles and surface excess within the numerical error (see Appendix). Finally, we compare the interfacial tension increment with experimental data. At 1 mol/l, we almost quantitatively reproduce the experimental interfacial tensions and in specific capture the Hofmeister trends: the larger ions show a weaker increase of interfacial tension and thus less repulsion from the interface. This transpires when comparing NaI with NaF or when comparing CsCl with LiCl. Interestingly, for Li we correctly observe the reversal of the Hofmeister trend, i.e., Li is less repelled from the interface than the larger Na ion. This effect we rationalize by the strong binding of the first solvation shell of water, which makes Li appear larger. Our conclusion from the simulation results is that non-polarizable ionic force fields that are rationally optimized with respect to thermodynamic bulk properties seem to capture interfacial effects quite well. The stronger interfacial activity of the larger halide ions is described by an adapted version of the theory of hydrophobic solvation developed in the context of neutral solutes [30]. According to that theory, the free energy cost to solvate a small neutral cavity scales with the cavity volume. Since iodide is by far the largest of all ions considered by us, this suggests that adsorption of iodide at the air/water interface is dominated by its partially hydrophobic nature.

2. Methods

2.1. Potentials of mean force (PMFs) of non-polarizable ions at the air/water interface

Simulations are performed in a rectangular box of 30 Å × 30 Å × 90 Å. A slab of water comprised of 2670 water molecules is placed

Table 1
Lennard-Jones parameters of the non-polarizable force fields used for the description of ions in the molecular dynamics simulations. The parameters are optimized such that they reproduce the solvation thermodynamics in a consistent manner, choosing chloride as a reference ion described by the Smith–Dang parameters [28]. For cations, an unambiguous determination of the parameters is not possible, and three different parameter sets are used, for details see Ref. [26]. The labeling of the parameter sets is identical to Figs. 1 and 2. σ_{IW} is given in units of Å, and ε_{IW} is given in units of kJ/mol.

Ion	Set 1		Set 2		Set 3		Set 4	
	σ_{IW}	ε_{IW}	σ_{IW}	ε_{IW}	σ_{IW}	ε_{IW}	σ_{IW}	ε_{IW}
Li	2.27	1.00	2.32	0.65	3.02	0.02		
Na	2.65	1.00	2.70	0.65	3.49	0.02		
K	2.97	1.00	3.03	0.65	3.85	0.02		
Cs	3.25	1.00	3.30	0.65	4.17	0.02		
F	3.30	0.55						
Cl	3.78	0.52						
Br	4.00	0.37						
I	4.25	0.32	4.09	0.80	4.25	0.50	4.09	0.53

in the simulation box that spontaneously forms two air/water interfaces normal to the z-axis, and one water molecule is replaced by an ion. The simulations are done at a temperature of 300 K in the *NVT* (constant number of particles, volume, and temperature) ensemble. Periodic boundary conditions are applied, and long-range Coulomb forces are calculated using particle-mesh Ewald summation [31]. A cutoff radius of 11 Å is used for the van der Waals interactions. We calculate the PMFs for ion adsorption at the air/water interface. The studied ions are the alkali metal cations Li^+, Na^+, K^+, Cs^+, and the halide anions F^-, Cl^-, Br^-, and I^-. The water model used is the extended simple point charge (SPC/E) model [25], and the ion parameters, which are shown in Table 1, were previously optimized for reproducing thermodynamic bulk solvation properties within molecular dynamics simulations [26]. In order to gain a feeling for the sensitivity of surface properties on the ionic force fields employed, for iodide, we calculate the PMF for three additional parameter combinations, also shown in Table 1 and Fig. 1. The original parameters for iodide (set 1) reproduce the solvation free energy and the solvation entropy of iodide. Set 2 reproduces the solvation free energy and the first maximum of the ion-oxygen RDF. Set 3 reproduces only the first maximum of the ion-oxygen RDF, and set 4 reproduces only the solvation entropy. In addition to the simulations for ions, we also calculate the PMFs for neutral particles with Lennard-Jones parameters identical to a fluoride ion and an iodide ion as given in parameter set 1 in Table 1. All PMFs are calculated by umbrella sampling [32] (window spacing 0.25 Å, 1 ns simulation time), and WHAM [33]. In every simulation the ion-oxygen RDF $g_{IW}(r)$ is obtained, from which the coordination number

$$n_c(r) = \int_0^r 4\pi r^2 g_{IW}(r')\,dr' \tag{1}$$

is derived. The average number of water molecules in the ion's first hydration shell is denoted as $n^1 = n_c(r^1)$, where r^1 is the position of the first minimum of the radial distribution function. In the evaluation of n^1 we assume that the position of the minimum of the radial distribution function does not depend on the ion's separation from the Gibbs dividing surface, which is very well satisfied. All simulations are performed with the GROMACS 3.3.1 [34] simulation package.

2.2. Simulations for polarizable ions

In the supplement we explain the methodology and show results for the bulk solvation free energy and the induced dipole distribution of polarizable ions (see Appendix).

2.3. Extended Poisson–Boltzmann equation

Our calculated PMFs are valid for infinite dilution only. The link to experimental data at finite concentration is achieved with an extended Poisson–Boltzmann (PB) approach, in which the PMF from MD simulations, V^{PMF}, is included. The extended PB equation for unpolarizable ions reads [8,35,36,10]

$$\epsilon_0 \frac{d}{dz}\epsilon_r(z)\frac{d}{dz}\Phi(z) = -\sum_i q_i c_i^{bulk} e^{-\left[V_i^{PMF}(z) - q_i\Phi(z)\right]/k_BT}, \tag{2}$$

where q_i is the charge of ions of type i, c_i^{bulk} is their bulk concentration, and ϵ_0 is the dielectric constant of vacuum. ϵ_r is the relative dielectric constant, which is assumed to be constant. The extended PB equation is solved numerically with the boundary conditions that the potential $\Phi(z)$ is (i) zero inside the water bulk ($z \to \infty$) and (ii) constant in the vapor phase ($z \to -\infty$). The numerical solution is performed on a one-dimensional grid with a lattice constant of 1 pm, for which discretization effects are negligible. Validation of the PB approach is done by comparison to MD simulation at a finite salt concentration of 0.85 mol/l, as explained in the supplement (see Appendix).

2.4. Surface tension

The surface tension change is obtained from the surface excess

$$\Gamma_i = \int_{-\infty}^{z_{GDS}} c_i(z)\,dz + \int_{z_{GDS}}^{\infty}\left[c_i(z) - c_i^{bulk}\right]dz, \tag{3}$$

where $c_i(z) = c_i^{bulk} e^{-[V^{PMF}(z) + q_i\Phi(z)]/k_BT}$ is the local concentration of species i as a function of z. The location of the Gibbs diving surface z_{GDS} is defined by the requirement that the surface excess of water, Γ_{wat}, vanishes. For a given bulk concentration c_i^{bulk}, the concentration profiles $c_i(z)$ are obtained self-consistently from the converged solution of the extended PB equation. The Gibbs equation relates the surface excess to the change in surface tension. For ideal solutions, i.e. assuming that the activities equal the concentrations, it reads

$$\Delta\gamma(c^{bulk}) = -k_BT\int_0^{c^{bulk}} dc^0 \sum_i \frac{\Gamma_i(c^0)}{c^0}. \tag{4}$$

Corrections due to the non-ideality of the solution are quite small and can be neglected for most practical applications [37]. The integration in Eq. (4) is performed numerically in steps of 0.01 mol/l.

3. Results and discussion

For all cation force-field parameters given in Table 1, the PMF for a single ion at the air/water interface is shown in Fig. 3a. All cations are repelled, there is no free energy minimum close to the interface. For every cation species, three different parameter sets are studied. For a given alkali ion, the PMFs obtained with $\varepsilon_{IW} = 0.65$ kJ/mol and $\varepsilon_{IW} = 1.0$ kJ/mol are very similar. The PMFs obtained with $\varepsilon_{IW} = 0.02$ kJ/mol differ more significantly from the two other ones. This shows that the interfacial properties of a cation are to a good approximation but not entirely determined

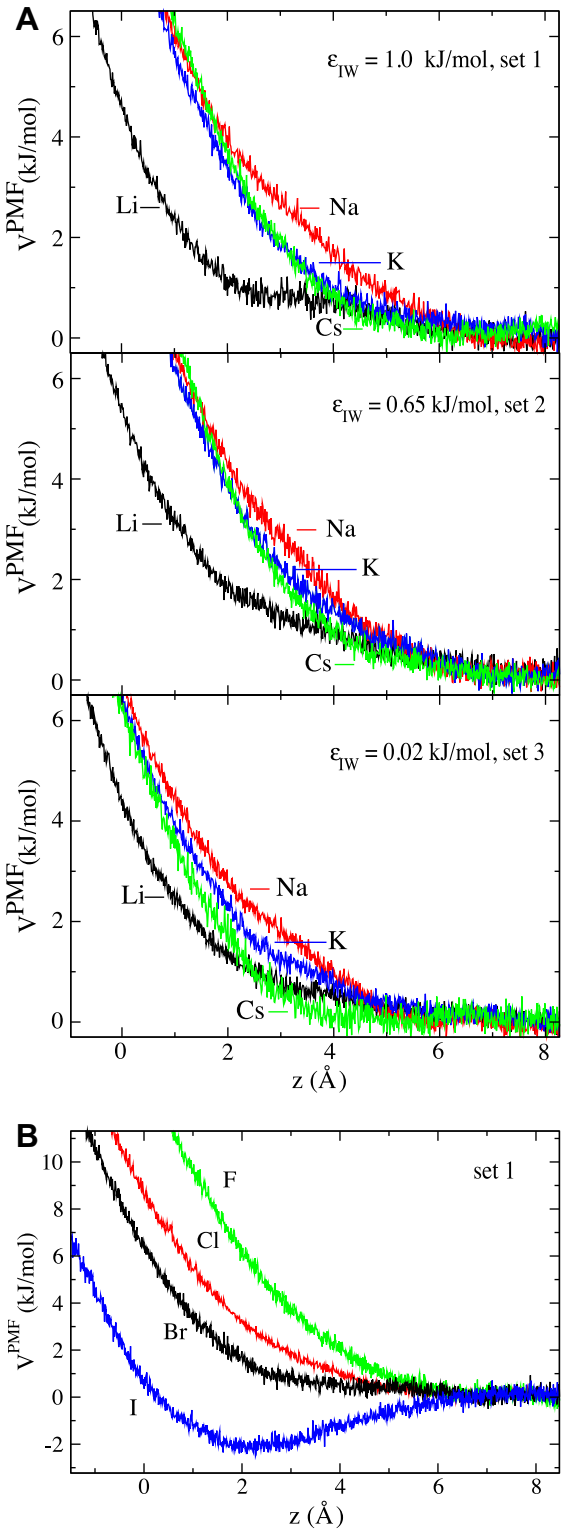

Fig. 3. Potentials of mean force at the air/water interface obtained by molecular dynamics simulations for (A) alkali metal cations with the parameter sets 1, 2, and 3 shown in Table 1 and (B) halide anions with the parameter set 1 used for iodide. All cation potentials of mean force are repulsive. For all three parameter sets, the repulsion of Li^+, the smallest cation, is significantly weaker than for the other cations. For the halides, there is a clear ordering of the potentials of mean force: the largest anion, iodide, is attracted to the interface, the smaller anions are increasingly repelled from the interface with decreasing ion size.

by its solvation free energy, which is identical for the three parameter sets. In fact, the trends are similar for the three force field sets: lithium, despite its small radius, feels the least repulsion from the interface. This observation is notable, because the image repulsion an ion experiences at the air/water interface is, according to a simple dielectric continuum model, strongest for small ions [38]. Sodium, the second smallest cation, feels the strongest repulsion. For the larger potassium ion, the repulsion is weaker than for sodium, but slightly larger than for cesium, the biggest cation in our study. The unexpected behavior of lithium is related to its strongly bound first solvation shell of water. To explore this further, in Fig. 4, we show the average number of water molecules in the first solvation shell of all cations, n^1, as a function of the ion's separation from the interface. For lithium, the first solvation shell stays intact for all separations from the interface. For the larger cations, the first solvation shell partially dissolves as they approach the interface: n^1 decreases steadily as the ions get closer to the Gibbs dividing surface. Thus, in our simulations we observe the PMF of a fully solvated lithium, which has an effectively large radius, while the PMFs of the larger cations takes the gradual degradation of the solvent shell as the ions approach the interface into account. It seems plausible that a continuum model based on a dielectric sphere corresponding to the bare ionic radius breaks down for the larger cations, in line with our simulation results.

For the anions described by parameter set 1 in Table 1, the PMFs are shown in Fig. 3b. The large iodide ion is considerably attracted to the air/water interface: there is a 2 kJ/mol deep minimum in the PMF 2 Å away from the Gibbs dividing surface. We do not observe a minimum in the PMFs for the smaller halide ions. Bromide, chloride and fluoride are increasingly repelled from the interface with decreasing distance to the GDS. This behavior qualitatively agrees with polarizable force field simulations, but we note that the surface enhancement we observe for iodide is much milder than previously obtained for polarizable force fields [16,43]. In fact, our results for non-polarizable force fields seem to suggest that ionic polarizability is not essential for iodide to adsorb to the air/water interface, in agreement with other recent simulation studies [21–23].

In order to gain understanding of the mechanisms involved in the surface activity of the large halide ions, we turn to neutral particles for the moment. In Fig. 5b we show the PMFs for neutral particles with the Lennard-Jones parameters corresponding to fluoride and iodide ions. In this figure, we also show as solid lines the predictions from a simple theory for the solvation free energy of a hydrophobic spherical cavity as a function of the separation from the air/water interface. This theory is a generalization of the so-called information theory approach to hydrophobic solvation in bulk [30]. According to that theory, the solvation free energy of a hard-sphere cavity of radius R is essentially equal to the logarithm of the probability of spontaneously forming a void matching the cavity volume. In the supplement we apply the information theory approach to SPC/E water and show that the bulk solvation free energy for the radii of interest in the current context can be accurately described by the expression $\mu_{ex} = \xi 4\pi R^3/3$ and thus is proportional to the cavity volume, as shown previously [30]. The prefactor for SPC/E water is given by $\xi = 0.195\ \mathrm{kJ/mol\ Å^{-3}}$ (see Appendix). Following the idea of Bocquet and coworkers [22], we model the solvation free energy of a sphere that partially penetrates the air/water interface as proportional to the fraction of its volume that is still immersed in water. For a sharp air/water interface located at $z = 0$ and a sharply defined cavity surface of radius R, the z-dependent solvation free energy (with the reference state defined as the bulk solvated state) thus reads

$$V^0_{cav}(z)/\xi = \begin{cases} -\frac{4\pi}{3}R^3 & z < -R, \\ -\frac{2\pi}{3}R^3 + \pi R^2 z - \frac{\pi}{3}z^3 & -R < z < R, \\ 0 & z > R. \end{cases} \quad (5)$$

However, both the planar air/water interface and the water interface surrounding the spherical cavity are rough. The intrinsic

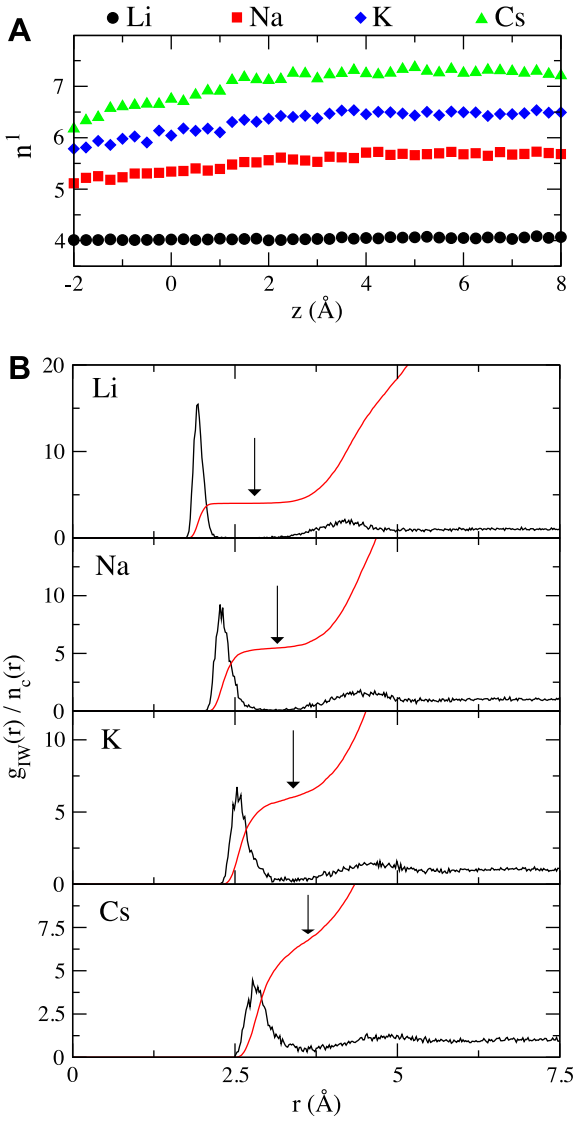

Fig. 4. (A) Cation coordination number in the first solvation shell, n^1, as defined in Eq. (1), as a function of its distance z from the Gibbs dividing surface. Simulations are done with the cationic parameter set 3. (B) Radial distribution function $g_{IW}(r)$ and coordination number $n_c(r)$ for Li^+, Na^+, K^+, and Cs^+ obtained from simulations with the parameter set 3 ($\varepsilon_{IW} = 0.02$ kJ/mol) for $z = 8.5$ Å. The arrows indicate the positions of the first minimum of $g_{IW}(r)$, which defines the number of water molecules in the first solvation shell, n^1. The steady decrease of the first shell coordination number n^1 for Na^+, K^+, and Cs^+ as the ion gets closer to the interface indicates reduced ion hydration. In contrast, the first solvation shell of Li^+ stays intact. This intuitively explains the finding that lithium feels the least repulsion from the interface of all cations. The ion radii (the first maximum of $g_{IW}(r)$) are 1.91 Å (Li), 2.28 Å (Na), 2.54 Å (K), and 2.79 Å (Cs).

interfacial broadness of the planar air/water interface leads to a smeared-out normalized density profile $\bar{\rho}(z) = 0.5[1+\tanh(2z/w)]$, where the intrinsic width $w = 3.3$ Å was recently extracted from MD simulations [39]. Since the smearing of the solvation interaction involves the simultaneous influence of two interfaces, we take as an effective width twice that value, i.e. $w = 6.6$ Å. The solvation energy at the broadened interfaces is then given by the convolution

$$V_{cav}(z) = \int_{-\infty}^{\infty} V^0_{cav}(z')\bar{\rho}'(z - z' - \Delta z)\mathrm{d}z', \qquad (6)$$

where the shift Δz accounts for a deformation of the planar air/water interface due to the presence of a particle or ion close to the interface and $\bar{\rho}'(z) = \mathrm{d}\bar{\rho}(z)/\mathrm{d}z$. For the effective radii R of the cavities we use the first maximum in the ion-oxygen RDF,

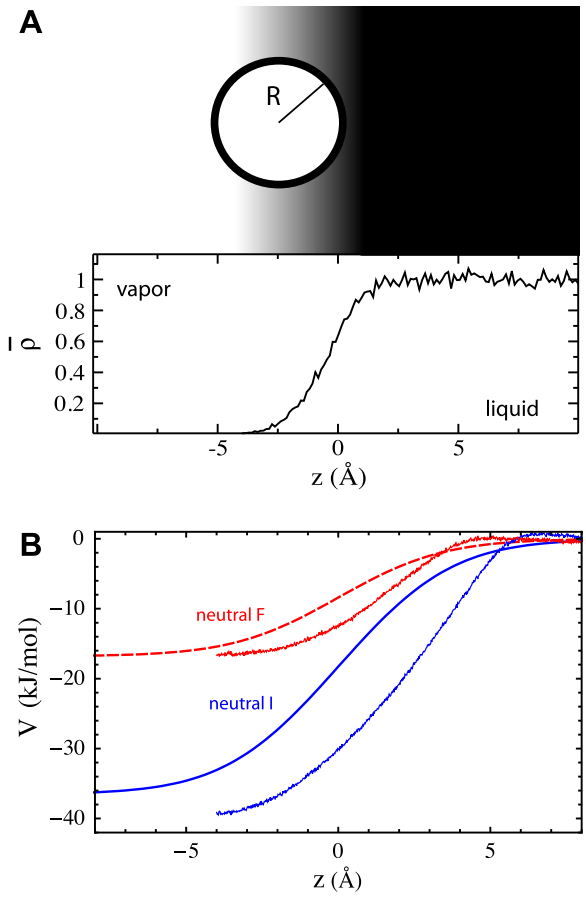

Fig. 5. (A) Schematic picture of the solvation of a hydrophobic sphere of radius R that partially penetrates the vapor/liquid interface. The inset shows the actual water density profile $\bar{\rho}(z)$ from the simulation. (B) Potentials of mean force for adsorption of neutral Lennard-Jones particles with parameters of fluoride and iodide. Shown are simulation results (noisy curves) and theoretical results from the adapted hydrophobic solvation theory, Eq. (6), without accounting for a deformation of the air–water interface, i.e. $\Delta z = 0$. The cavity radii R for the theoretical estimates are obtained from the position of the first maximum in the corresponding ion-water radial distribution function, $R_F = 2.74$ Å and $R_I = 3.55$ Å, further details are given in the supplement (see Appendix). The qualitative agreement is good.

$R_F = 2.74$ Å and $R_I = 3.55$ Å, details are given in the supplement (see Appendix). Fig. 5b shows that the theoretical solvation interaction Eq. (6) (where we put $\Delta z = 0$ for the moment) gives a good estimate of the actual PMF of uncharged particles. In the simulations, the free energy drops by 16 kJ/mol when a 'neutral fluoride' particle leaves the water phase, very close to what is obtained from Eq. (6). For the 'neutral iodide' particle the free energy change in the simulation (−39 kJ/mol) is slightly underestimated by Eq. (6) (−36 kJ/mol). Allowing for a shift of the interface position via the parameter Δz is justified since the presence of a hydrophobic particle close to the interface leads to considerable interface deformation. In Fig. 7 we show snapshots from simulations of iodide and fluoride ions and their neutral counterparts at the air/water interface. The largest interface deformation is observed for the neutral iodide species in (c), but even the charged iodide species in (a) shows considerable deformation. The effect is reduced but still visible for the smaller neutral fluoride species in (d), and only for the charged fluoride ion in (b), there is no visible bending of the interface. The ion keeps an intact first solvation sphere upon approach to the interface, which demonstrates the strong water binding affinity of the small fluoride ion. What we directly appreciate from these snapshots is that even the charged iodide ion behaves as a hydrophobic particle when it approaches the interface and sheds off a large fraction of its water hydration shell.

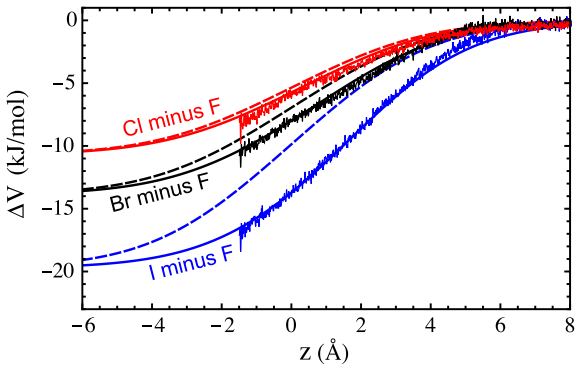

Fig. 6. Difference in potential of mean force at the air/water interface, $\Delta V_X = V_X - V_F$, relative to fluoride of chloride (red), bromide (black), and iodide (blue). The three noisy curves are the differences derived from the simulation data for the charged ions (shown in Fig 3). The smooth curves are the differences derived from the hydrophobic solvation theory for neutral particles adapted to the interfacial geometry, Eq. (6). The dashed lines are obtained without shifting the interface ($\Delta z = 0$), the full lines are obtained with shifts of $\Delta z = 0.1$ Å (chloride), $\Delta z = 0.25$ Å (bromide), and $\Delta z = 0.8$ Å (iodide). The shift for fluoride is zero. The cavity radii R for the theoretical estimates are obtained from the position of the first maxima in the corresponding ion-water radial distribution function, $R_F = 2.74$ Å, $R_{Cl} = 3.23$ Å, $R_{Br} = 3.35$ Å and $R_I = 3.55$ Å, further details are given in the supplement (see Appendix).

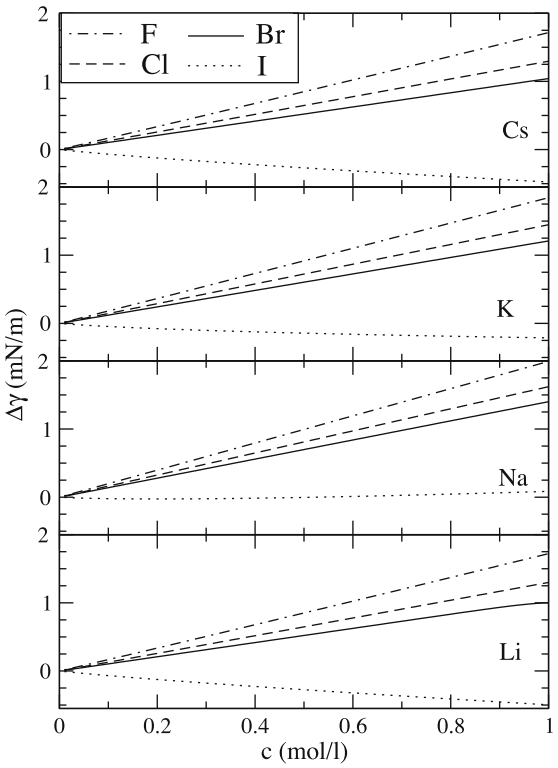

Fig. 8. Interfacial tension increment at the air/water interface as a function of the salt concentration for alkali halides obtained from the Gibbs adsorption equation, Eq. (4), in conjunction with the extended Poisson–Boltzmann equation, Eq. (2). The input for the extended Poisson–Boltzmann equation are analytical fit expressions of the potentials of mean force from the simulations in Fig. 3 (see Appendix). The force fields used are the parameter sets 1 (anions) and 3 (cations).

For charged ions at the air/water interface, the question now is whether the hydrophobic solvation of uncharged species, studied in Fig. 5, can explain the interfacial activity observed with iodide. To separate effects due to the ion's charge, which are less ion-specific than the strongly ion radius dependent hydrophobic solvation effects, we subtract the fluoride PMF from the other halide PMFs. In Fig. 6 we show these differential PMFs, $\Delta V_X = V_X - V_F$, for Cl, Br, and I. Since the small fluoride ion feels the strongest repulsion at the air/water interface, ΔV_X is increasingly negative for Cl, Br, and I. Also shown are the corresponding differences of the theoretical predictions according to Eq. (6), using the corresponding ionic radii R and for zero shift $\Delta z = 0$ (broken lines). The theoretical predictions account reasonably for the differential PMFs of the anions. Note also that the results for uncharged and charged species are comparable, lending support to the idea that the ion-specific difference of the halide PMFs is due to hydrophobic solvation effects. The agreement between Eq. (6) and the MD results becomes nearly ideal, when we allow for a finite shift Δz of the interfacial solvation potential. In Fig. 6 we also show the predictions for the differential PMFs according to Eq. (6) with a fitted shift $\Delta z = 0.8$ Å for iodide, $\Delta z = 0.25$ Å for bromide, and $\Delta z = 0.1$ Å for chloride as solid lines (while the shift for fluoride was assumed to vanish). This shows that the ion-specific part of the interaction of anions with the air/water interface, which we single out by looking at the difference between the PMFs of two different ions, is well-described by standard hydrophobic solvation theory that is adapted to the interfacial geometry. We conclude that polarizability effects most likely have only a small influence on the interfacial activity of ions, and in specific are not responsible for the ion-specificity of

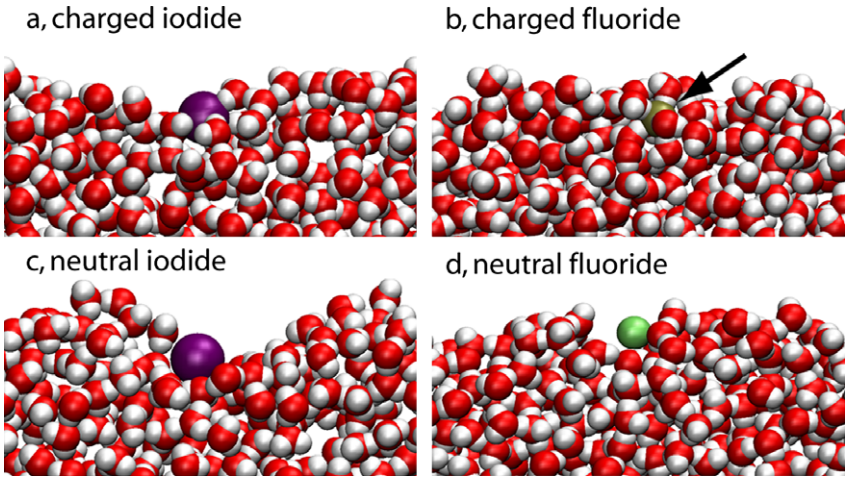

Fig. 7. Snapshots of simulations of (a) an iodide ion, (b) a fluoride ion, (c) a neutral particle with the Lennard-Jones parameters of iodide, and (d) a neutral particle with the Lennard-Jones parameters of fluoride. The snapshots are taken from simulations in which the ion is restrained to a position 2.5 Å away from the Gibbs dividing surface in the water phase. In snapshots (a) and (c) it is seen that iodide bends the interface in the neutral and (weaker) in the charged version. For the smaller neutral fluoride in (d) the interface bending is only weak, and for the charged fluoride in (b) bending is completely absent.

interfacial ion adsorption. This conclusion was also reached based on previous simulations employing polarizable force fields for ions at hydrophobic substrates [10] and will be discussed in more detail further below.

In Fig. 8 we show the interfacial tension increment with respect to the bare air/water interface as a function of salt concentration for all possible ion combinations using the alkali force field set 3, calculated according to the extended PB Eq. (2) and the Gibbs equation (4). The PB approximation is a mean-field approach that is known to fail both for highly concentrated salt solutions because of the neglect of excluded-volume interactions and for highly charged ions because of the neglect of correlation effects [40]. In order to check that the approximations inherent in the PB formalism do not lead to drastic errors, we calculated ion concentration profiles at finite concentration $c^{bulk} = 0.85$ mol/l for NaI and NaBr both within the extended PB formalism and by MD simulations (see supplement). The statistical fluctuations of the MD concentration profiles are considerable even after 100 ns simulation runs, in contrast to previous MD simulations employing polarizable force fields [18,41]; the reason for this is that the PMFs in the present case show a much less pronounced minimum for iodide and no minimum at all for bromide and thus the concentration variations in the profile are very moderate. Nevertheless, MD simulation and PB concentration profiles agree quite well which serves as a validation of our extended PB procedure (see Appendix). Note that the $c^{bulk} = 0.85$ mol/l case is an upper estimate of the expected deviations between MD and PB, since the concentration profiles by definition become identical as one approaches the infinite-dilution limit. The interfacial tension increments in Fig. 8 exhibit a nearly linear dependence on the salt concentration, in agreement with experimental results [42], the slopes of which correlate in a quite intuitive manner with the PMFs in Fig. 3. The less repulsive the PMF for the anion, the smaller the slope of the interfacial tension becomes; for iodide this even leads to negative interfacial increments for LiI, KI and CsI. To quantitatively relate to experiments, in Fig. 9 we compare our PB predictions for the interfacial tension increment at $c^{bulk} = 1$ mol/l for (a) sodium halide solutions and (b) alkali chloride solutions with experimental data [42]. The comparison is almost quantitative, the Hofmeister trend as the ion size increases is well captured, and even the anomaly of the lithium chloride interfacial tension, which is smaller than the surface tension of a sodium chloride solution, is reproduced. The only glitch is NaF, for which we predict a larger tension than for NaCl, in contradiction to the experimental situation. This failure is not surprising, as the parameter optimization for fluoride did not work as well as for Br, Cl and I due to the non-crossing between the energy and entropy solvation curves (see Fig. 1). The variance between the three different alkali force fields, denoted by the open symbols in Fig. 9, is quite small, considering the vast difference of the actual Lennard-Jones parameter between the three alkali parameter sets (compare Fig. 2). The overall agreement between our predictions and the experimental data gives not only confidence into our force-field optimization strategy, it also suggests that the force fields, which are optimized in bulk, are transferable to interfacial

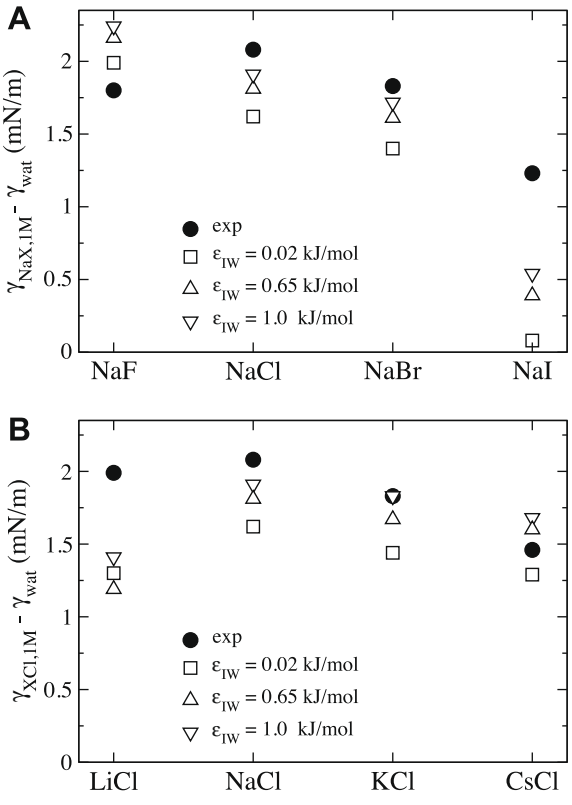

Fig. 9. (A) Interfacial tension increment of sodium halide solutions at concentration 1 mol/l. (B) Interfacial tension increment of 1 mol/l alkali chloride solution. Full circles show experimental data from Ref. [42], the open symbols show our predictions obtained by the extended Poisson–Boltzmann modeling. For the sodium halides, the qualitative trend that the surface tension becomes smaller for the series Cl–Br–I is reproduced. The experimental results of the alkali chloride solutions show a maximum in the surface tension for sodium. This maximum is reproduced by our modeling results.

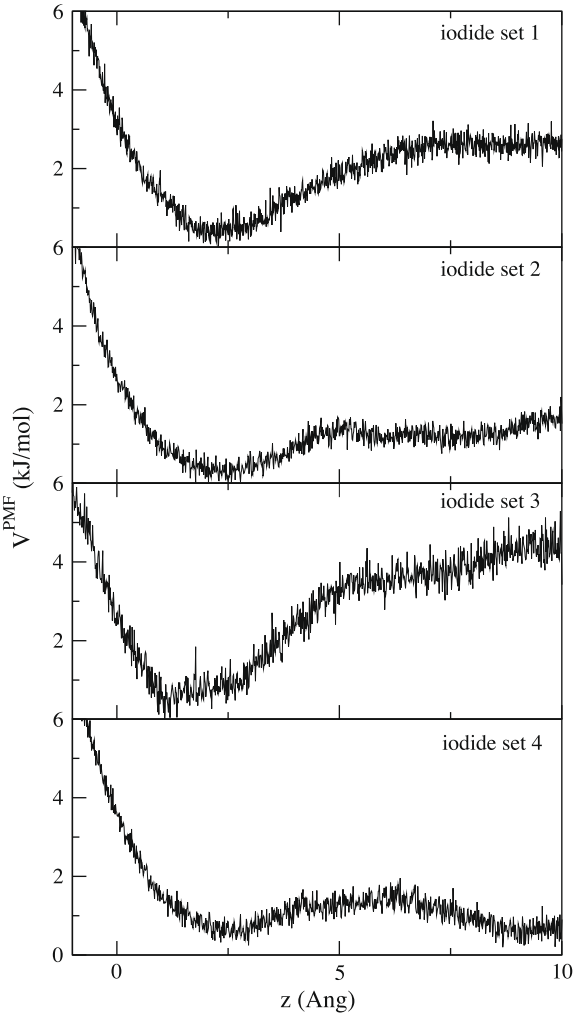

Fig. 10. Potentials of mean force for iodide at the air/water interface based on four different trial parameter combinations shown in Fig. 1. The four potentials of mean force differ significantly.

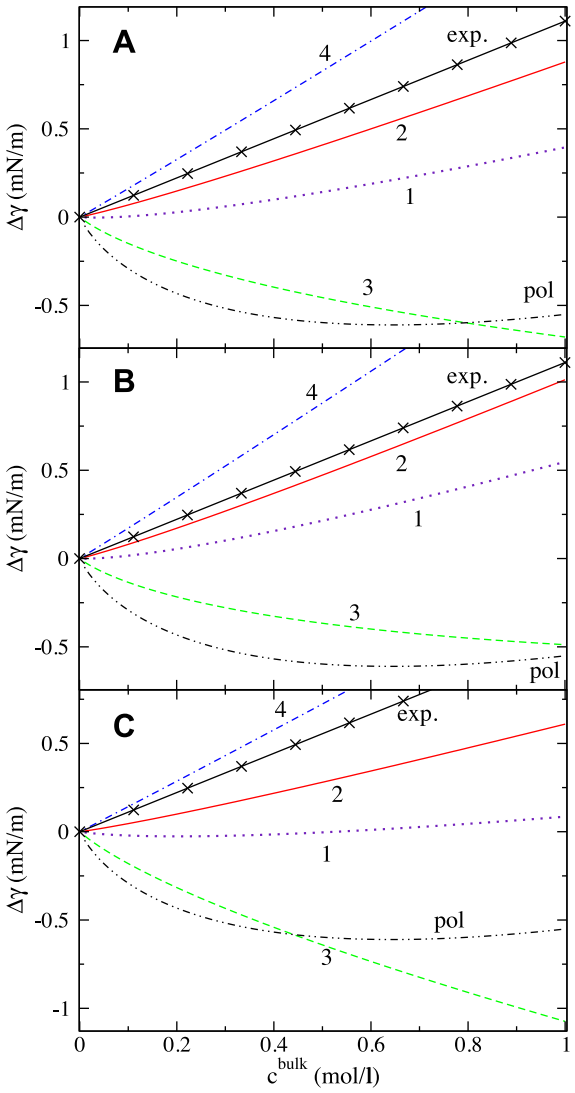

Fig. 11. Incremental interfacial tension for NaI. The sodium parameter is taken from: (A) parameter set 1 in Table 1 ($\varepsilon_{iW} = 1.0$ kJ/mol), (B) set 2 ($\varepsilon_{iW} = 0.65$ kJ/mol), and (C) set 3 ($\varepsilon_{iW} = 0.02$ kJ/mol). Results for the four different iodide trial parameter sets, denoted by numerals 1, 2, 3, 4, as indicated in Fig. 1, are shown. The interfacial tension is calculated from the Gibbs adsorption equation (Eq. (4)) and the extended Poisson–Boltzmann equation (Eq. (2)). Also shown is the interfacial tension from previous simulations with polarizable ion parameters [43,10] (dashed-double dotted line) and the experimental data (solid line with crosses).

situations. This transferability of bulk-optimized force fields is a priori not guaranteed but clearly of great importance, because it implies that non-polarizable force fields should be able to correctly model ion-specific situations where ions are present both at interfaces and in bulk (the normal situation for simulations involving, e.g. protein surfaces). For the alkali metal cations, the interfacial adsorption strength seems to be largely invariant with respect to the position along the constant solvation free energy curve, which leaves the freedom to potentially optimize the force-field parameters with respect to some additional experimental observable.

The largest error is obtained for NaI; to look into this issue and at the same time investigate the sensitivity of interfacial ionic adsorption on force-field variations, we show in Fig. 10 the PMFs for the four different trial iodide parameter sets indicated in Fig. 1. In Fig. 11 we show the interfacial tension increments as a function of salt concentration. For comparison, we also show results obtained previously for polarizable force fields [43,10]. Set 1, which reproduces the solvation free energy and the solvation entropy, underestimates the interfacial tension. Set 3 gives an even lower interfacial tension, which is not a surprise as the PMF exhibits a more pronounced minimum than set 1 (see Fig. 10). Sets 2 and 4 yield the best agreement with the experimental interfacial tension data. Sets 1 and 2 yield the same solvation free energy of iodide and the actual Lennard-Jones parameters differ only very little, yet they predict a quite different interfacial affinity as judged from the PMFs and interfacial tensions. This is quite different from alkali cations, where wide force-field variations along the constant solvation free energy line only lead to moderate interfacial tension changes. This means that a further refinement of ionic force-field parameters with respect to interfacial affinity is in principle possible, especially for the case of anions. The polarizable NaI force-field parameters predict a negative interfacial tension increment, see Fig. 11, in contrast to experimental data, which is caused by a strongly attractive minimum in the PMF with a depth of more than 6 kJ/mol [43]. We conclude that the polarizable force fields describe the interfacial affinity of iodide less accurate than our bulk-optimized non-polarizable force fields.

4. Conclusions

We describe the use of recently bulk-optimized non-polarizable ion parameters for the study of adsorption properties at the air/water interface. The surface affinity of iodide turns out to be quite small, and exhibits an attractive minimum in the potential of mean force of only about 2 kJ/mol. The difference of the interfacial affinity between the halide anions, i.e. the ion-specific contribution, can be explained by an interface-adapted version of the standard theory of hydrophobic solvation. Since the interfacial affinities are quite small, straight MD simulations at finite concentrations are not able to yield properly converged concentration profiles and therefore cannot be used to calculate interfacial tensions according to the Gibbs equation. We therefore employ an extended Poisson–Boltzmann equation based on the simulated ionic potentials of mean force. The calculated interfacial tensions agree almost quantitatively with experimental data and capture the Hofmeister trend as well as the anomalous behavior of lithium. We conclude that properly bulk-optimized ionic force fields are transferable to interfacial situations and we thus explicitly demonstrate the linkage between bulk and interfacial Hofmeister ion-specific effects for the (admittedly simple) case of the air/water interface.

We finally comment on the performance of polarizable versus non-polarizable force fields in the context of interfacial electrolyte simulations. Although the orientational polarizability of water is much larger than its atomic polarizability, there is no doubt that atomic polarization occurs and is important especially for water and ions that are close to other small ions. In fact, quantum chemistry calculations demonstrate that polarizability effects give, e.g., for NaCl a sizeable contribution to the ion–ion interaction energy of about 25 kJ/mol in vacuum and alone are sufficient to explain the ionic binding energy without the need to invoke additional quantum-chemical effects [44]. On a more simplistic level, a polarizable force field with three adjustable parameters should allow for a more faithful description of reality than a non-polarizable force field with just two parameters. Nevertheless, the polarizable ionic force field from literature that we have tested is not well-optimized and proves inferior to well-optimized non-polarizable force fields. As shown in detail in the supplement, the solvation free energies of sodium halides obtained with the polarizable force field [43] are off from experimental values by typically 40 kJ/mol, whereas our optimized non-polarizable force fields bring that error down to about 1 kJ/mol (see Appendix). In light of this, it is not surprising that the interfacial tension increment of NaI at 1 mol/l comes out qualitatively wrong with the polarizable force field, as shown in Fig. 11. Furthermore, if damping schemes are used in

polarizable force-field simulations to avoid the polarization catastrophe, an additional force-field parameter is introduced that can, in extreme cases, decisively influence the simulation results, as we show in the supplement (see Appendix). It is often argued that ions with a large polarizability preferentially adsorb on aqueous interfaces because of the pronounced electric fields associated with interfacial water dipole orientations, for a detailed discussion see Ref. [45]. Besides the fact that hydrophobic solvation effects alone are sufficient to explain the interfacial activity of, e.g. iodide observed in the simulations (as we show in this Letter), this argument is seriously flawed, as the excess polarizability (i.e. the difference between the ion's polarizability and the polarizability of the displaced water) is negative [44]. Previous comparisons between the performance of polarizable and non-polarizable force fields in interfacial geometries used inferior non-polarizable force field parameters and therefore have only limited suggestive power. Likely, this will change in the future when rigorously optimized polarizable force fields are available.

Acknowledgements

We acknowledge financial support from the German Excellence Initiative via the Nanosystems Initiative Munich (NIM), the Elite Netzwerk Bayern (CompInt), the Deutsche Forschungsgemeinschaft (DFG Grant NE 801/4), and the Ministry for Economy and Technology (BMWi) in the framework of the AiF project 'Simulation and prediction of salt influence on biological systems'. L.V. thanks the Alexander von Humboldt Foundation for a Humboldt Fellowship. Sh.I.M. acknowledges support from the IDB Post-Doctoral Scholarship Program (36/1/339). The Leibniz Rechenzentrum Munich is acknowledged for supercomputing access.

Appendix A. Supplementary material

Supplementary data associated with this article can be found, in the online version, at doi:10.1016/j.cplett.2009.07.077.

References

[1] W. Kunz, P. Lo Nostro, B.W. Ninham, Curr. Opin. Colloid Interf. Sci. 9 (2004) 1.
[2] N.L. Jarvis, M.A. Scheiman, J. Phys. Chem. 72 (1968) 74.
[3] D. Liu, G. Ma, L.M. Levering, H.C. Allen, J. Phys. Chem. B 108 (2004) 2252.
[4] P.B. Petersen, R. Saykally, J. Ann. Rev. Phys. Chem. 57 (2006) 333.
[5] V. Padmanabhan, J. Daillant, L. Belloni, S. Mora, M. Alba, O. Konovalov, Phys. Rev. Lett. 99 (2007) 086105.
[6] L. Onsager, N.N.T. Samaras, J. Chem. Phys. 2 (1934) 528.
[7] V.S. Markin, A.G. Volkov, J. Phys. Chem. B 106 (2002) 11810.
[8] M. Boström, D.R.M. Williams, B.W. Ninham, Phys. Rev. Lett. 87 (2001) 168103.
[9] M.A. Wilson, A. Pohorille, L.R. Pratt, J. Phys. Chem. 91 (1987) 4873.
[10] D. Horinek, R.R. Netz, Phys. Rev. Lett. 99 (2007) 226104.
[11] C.Y. Lee, J.A. McCammon, P.J. Rossky, J. Chem. Phys. 80 (1984) 4448.
[12] M.A. Wilson, A. Pohorille, L.R. Pratt, Chem. Phys. 129 (1989) 209.
[13] J. Caldwell, L.X. Dang, P.A. Kollman, J. Am. Chem. Soc. 112 (1990) 9144.
[14] A. Wallqvist, Chem. Phys. 148 (1990) 438.
[15] L. Perera, M.L. Berkowitz, J. Chem. Phys. 95 (1991) 1954.
[16] P. Jungwirth, D. Tobias, J. Phys. Chem. B 105 (2001) 10468.
[17] T.M. Chang, L.X. Dang, Chem. Rev. 106 (2006) 1305.
[18] P. Jungwirth, D. Tobias, J. Chem. Rev. 109 (2006) 1259.
[19] M.A. Wilson, A. Pohorille, L.R. Pratt, J. Chem. Phys. 90 (1989) 5211.
[20] L. Vrbka, M. Mucha, B. Minofar, P. Jungwirth, E.C. Brown, D.J. Tobias, Curr. Opin. Colloid Interf. Sci. 9 (2004) 67.
[21] S. Pal, F. Müller-Plathe, J. Phys. Chem. B 109 (2005) 6405.
[22] D. Huang, C. Cottin-Bizonne, C. Ybert, L. Bocquet, Langmuir 24 (2008) 1442.
[23] B. Eggimann, J. Siepmann, J. Phys. Chem. C 112 (2008) 210.
[24] K. Kudin, R. Car, J. Am. Chem. Soc. 130 (2008) 3915.
[25] H.J.C. Berendsen, J.R. Grigera, T.P. Straatsma, J. Phys. Chem. 91 (1987) 6269.
[26] D. Horinek, S.I. Mamatkulov, R.R. Netz, J. Chem. Phys. 30 (2009) 124507.
[27] M.A. Kastenholz, P.H. Hünenberger, J. Chem. Phys. 124 (2006) 124106.
[28] D.E. Smith, L.X. Dang, J. Chem. Phys. 100 (1994) 3757.
[29] A. Serr, R.R. Netz, Int. J. Quantum Chem. 106 (2006) 2690.
[30] G. Hummer, S. Garde, A.E. Garcia, A. Pohorille, L.R. Pratt, PNAS 93 (1996) 8951.
[31] U. Essmann, L. Perera, M.L. Berkowitz, T. Darden, H. Lee, L.G. Pedersen, J. Chem. Phys. 103 (1995) 8577.
[32] G.M. Torrie, J.P. Valleau, J. Comput. Phys. 23 (1977) 187.
[33] S. Kumar, J.M. Rosenberg, D. Bouzida, R.H. Swendsen, P.A. Kollman, J. Comput. Chem. 16 (1995) 1339.
[34] D. van der Spoel, E. Lindahl, B. Hess, G. Groenhof, A.E. Mark, H.J.C. Berendsen, J. Comput. Chem. 26 (2005) 1701.
[35] G. Luo et al., Science 311 (2006) 216.
[36] G. Luo et al., J. Elanal. Chem. 593 (2006) 142.
[37] D.J.V.A. dos Santos, F. Müller-Plathe, V.C. Weiss, J. Phys. Chem. C 112 (2008) 19431.
[38] Y.I. Kharkats, J. Ulstrup, J. Elanal. Chem. 308 (1991) 17.
[39] F. Sedlmeier, D. Horinek, R.R. Netz, in preparation.
[40] H. Boroudjerdi, Y.-W. Kim, A. Naji, R.R. Netz, X. Schlagberger, A. Serr, Phys. Rep. 416 (2005) 129.
[41] D. Horinek, A. Serr, D.J. Bonthuis, M. Boström, W. Kunz, R.R. Netz, Langmuir 24 (2008) 1271.
[42] P.K. Weissenborn, R.J. Pugh, J. Colloid Interf. Sci. 184 (1996) 550.
[43] L.X. Dang, J. Phys. Chem. B 106 (2002) 10388.
[44] R.R. Netz, Curr. Opin. Colloid Interf. Sci. 9 (2004) 192.
[45] G. Archontis, E. Leontidis, Chem. Phys. Lett. 420 (2006) 199.

Dominik Horinek studied chemistry at the University of Regensburg, where he obtained his Ph.D. in physical chemistry in 2000. After Postdocs at the University of Colorado at Boulder and at the Czech Academy of Sciences in Prague, he joined the bio soft matter physics group of Roland Netz at the Technical University of Munich, where he is working on his Habilitation.

Alexander Herz, a former professional software developer, is a student of biophysics at the Technical University of Munich in Germany. For his diploma thesis, he is working with Dominik Horinek on molecular dynamics simulations of aqueous interfacial systems.

Lubos Vrbka obtained his Ph.D. in physical chemistry in 2007 from the Charles University in Prague, after studies at the Institute of Organic Chemistry and Biochemistry of the Czech Academy of Sciences under the guidance of Profs. Pavel Jungwirth and Petr Nachtigall. He is now working as a Fellow of the Alexander von Humboldt Foundation at the University of Regensburg. His research focuses on theoretical studies of specific ion effects by means of computer simulations and statistical thermodynamics.

Felix Sedlmeier obtained his diploma in physics in 2008 from Technical University of Munich, Germany. Currently, he is working on his Ph.D. in the group Roland Netz at Technical University of Munich. His research interests include the structure and dynamics of water at interfaces and implications of hydrophobic hydration on protein stability.

Shavkat Mamatkulov received his B.Sc. in physics from the Tashkent State University (National University of Uzbekistan). He completed his Ph.D. in physics at the Heat Physics Department of the Uzbekistan Academy of Sciences in 1997. He is currently head of the computational chemistry group at the Heat Physics Department. In 2003 and 2006, he was a visiting scientist in the group of Roland Netz.

Roland R. Netz studied physics at the Technical University of Berlin and at MIT, and received his Ph.D. in 1994 from the University of Cologne. After postdocs at Tel- Aviv University, UCSB, Seattle, Institute Charles Sadron in Strasbourg and CEA in Paris, he was a research associate at the Max-Planck Institute for Colloids and Interfaces in Potsdam. He was appointed as an Associate Professor of physics at the LMU Munich in 2002. Since 2004 he has held a chair in bio-soft matter physics at the Technical University of Munich.